Pulsed Laser Deposition of NiSe$_2$ Film on Carbon Nanotubes for High-Performance Supercapacitor

Rongrong Nie,[1] Qunlong Wang,[2] Peng Sun,[1] Ruijing Wang,[1] Qin Yuan[1] and Xuefeng Wang[1*]

Amorphous NiSe$_2$ was deposited on the carbon nanotubes (CNTs) networks by the pulsed laser deposition method forming the CC@CNT@NiSe$_2$ composites. The CC@CNT@NiSe$_2$ electrode exhibits a high specific capacitance of 696 F g^{-1} at 2 A g^{-1} and the specific capacitance retention of 74 % in the long life test. To evaluate the practicality of our electrode, we assembled the CC@CNTs@NiSe$_2$//CC@CNTs asymmetric supercapacitor using CC@CNTs@NiSe$_2$ as positive electrode and CC@CNTs as the negative electrode, which shows an energy density of 11.9 Wh kg^{-1} at a power density of 242 W kg^{-1}. This work highlights the advantageous electrochemical performance of NiSe$_2$ film on CNTs, in which the highly conductive CNTs provide plentful electronic conduction channels and the NiSe$_2$ film exposures more active sites.

1. Introduction

The energy shortage has been a very serious problem in the world so that exploration of new energy storage equipment has become extremely urgent. Supercapacitors, known as electrochemical capacitors, have caused great concern due to its high power density, fast charging and excellent cycle stability.[1-3] The performance of supercapacitor strongly depends on the electrode materials,[4-6] among which nickel chalcogenides [7-9] attract more attention because of its unique electronic properties, large specific surface area and abundant chemical active sites. Recently, the charge storage mechanism and electrochemical properties of nickel oxides and sulfides have been extensively studied. Although nickel oxides[10, 11] has a high capacitance value, their ratio performance is poor with the occurrence of charge and discharge because of poor intrinsic conductivity. Nickel sulfides with a pyrite structure[12,13] are semiconductor that shows good electronic, optical and magnetic properties. Lu *et al.*[14] successfully synthesized NiS$_2$ hollow spheres with an L-cysteine assisted hydrothermal method and the specific capacitance of the NiS$_2$ electrode was 1643 F g^{-1} at a current density of 1 A g^{-1}, which is certificated that nickel sulfides can be as an excellent supercapacitor electrode.

Nickel diselenide, as one of the nickel chalcogenides, is expected to have similar electrochemistry properties as nickel disulfides due to analogous molecular structure. The most common crystal form of nickel diselenide is cubic structure with a pyrite structure.[15] What's more, nickel diselenide has a lower band gap with a higher intrinsic electrical conductivity and a tunable electronic configuration.[16] Hence, NiSe$_2$

could be used for high-performance supercapacitor electrode materials. However, pure NiSe$_2$ is so easy aggregation during the preparation process, which inevitably affects electrochemical performance.[17] For example, hexapod-like nickel diselenide electrode, synthesized by a facile hydrothermal, exhibited only a specific capacitance of 75 F g^{-1} at 1 mA cm^{-1}.[18] Uniform hollow-structure of NiSe$_2$ based on NiS$_2$ hollow spheres was obtained, which showed specific capacitance of 341 F g^{-1} at 1 A g^{-1}.[14] It is interesting to note that truncated cube-like NiSe$_2$ on Ni foam was synthesized by a facile hydrothermal giving a specific capacitance as high as 1044 F g^{-1} at 3 A g^{-1}.[19]

The pulsed laser deposition (PLD) is a physical vapor deposition technique for thin film fabrication, which has been widely used to produce new materials, such as catalysis[20] and energy storage.[21] In this work, NiSe$_2$ film was prepared by PLD deposited on CC@CNTs to form composite materials. The CNTs,[22] as the excellent electrical conductor, provide abundant electron transport channels and act as nanotular backone for deposition of NiSe$_2$ film. The excellent electrochemical performance of the CC@CNTs@NiSe$_2$ can be attributed to the synergism between NiSe$_2$ and CNTs, which is promising materials for energy storage.

2. Experimental

Synthesis of the CC@CNTs

The carbon nanotubes (CNTs) were grown on carbon cloth (CC) via a chemical vapor deposition (CVD).[23-25] The carbon cloth (1 cm ×1 cm) (CC, Hong Kong Physicochemical Limited Company) was treated in ethanol and deionized water with ultrasonic to remove the surface impurities. The pretreated CC was soaked in catalyst solution which was made up of 0.1 M polyethylene glycol (PEG) (C.P., Sinopharm Chemical Reagent Co., Ltd.) and 0.1 M Ni(NO$_3$)$_2$ (A.R., Sinopharm Chemical Reagent Co., Ltd.) for overnight. The CC dried in air was placed in tube furnace. H$_2$ and C$_2$H$_2$ are respectively introduced into the furnace and the molar ratio of H$_2$ and C$_2$H$_2$ is 1:2 (total pressure is 1.8x10^4 Pa at room temperature), which was heated up to 550 $^\circ$C at a heating rate of 5 $^\circ$C min^{-1} and held at 550 $^\circ$C for 1 h, and then cooled

[1]*Shanghai Key Lab of Chemical Assessment and Sustainability, School of Chemical Science and Engineering, Tongji University, Shanghai 200092, China*
[2]*Shanghai Joyworld Innovative Materials Technology Co. LTD, Shanghai 200433, China*
***E-mail:** xfwang@tongji.edu.cn*

down to room temperature.

Synthesis of the CC@CNTs@NiSe₂

$NiSe_2$ was deposited on the as-prepared CC@CNTs by PLD. First, $NiSe_2$ was synthesized by hydrothermal method with Nickel nitrate hexahydrate ($Ni(NO_3)_2 \cdot 6H_2O$), selenium powder and hydrazine hydrate (80 wt%) following the reported method.[19] Then $NiSe_2$ was pressured into the target by a tablet bead machine. The deposition condition is described as follows. A Nd: YAG laser with a wavelength of 1064 nm and a frequency of 10 Hz was applied to ablate $NiSe_2$ that is deposited on CC@CNTs (1 cm ×1 cm) surface. The quality of deposition was controlled by laser energy and deposition time. $NiSe_2$ with an active mass of approximately 0.99 mg was obtained under the conditions of the laser energy density of 220 mJ cm^{-2} and deposition time of 20 min.

Characterization

The analysis of morphology and size was performed by field emission scanning electron microscopy (FESEM; Hitachi S-4800) and transmission electron microscopy (TEM; JEOL, JEM-2100). The nanostructure was analyzed by Raman spectra (Renishaw Invia, 514 nm laser under ambient conditions). XPS data was obtained using a ThermoFisher 250XI.

Electrochemical performance testing

The electrochemical properties were tested by standard three-electrode system, using the CC@CNTs@NiSe₂ as working electrode, Ag/AgCl as reference electrode and Pt wire as a counter electrode. The cyclic voltammetry (CV), EIS and galvanostatic charge/discharge (GCD) were tested in 1 M KOH aqueous solution by using a CHI-660D electrochemical workstation.

The specific capacitance can be obtained by the galvanostatic discharge curve according to the following formula:[26]

$$C = I \int U(t)\,dt / \Delta U^2 m$$

where C is the specific capacitance (F g^{-1}), I is the discharge current (A), U is the potential (V), which is the function of discharge time t (s),

ΔU is the potential window (V), and m is the loading mass of the electroactive materials (g).

The asymmetric supercapacitor was assembled by using CC@CNTs@NiSe₂ as anode and CC@CNTs as cathode for further analysis of its electrochemical performance and practical application. The cyclic voltammetry (CV), galvanostatic charge/discharge (GCD) and the long term cycling life tests were tested using a two-electrode system in 1 M KOH aqueous solution.

The specific energy density and power density were calculated according to the following formula (1) and (2):[27]

$$E = \frac{C_{cell,m}\Delta V^2}{2 \times 3.6} \tag{1}$$

$$P = \frac{E_{cell,m} \times 3600}{\Delta t} \tag{2}$$

where E is the energy density (Wh kg^{-1}), C_{cell} is the specific capacitance (F g^{-1}), ΔV is the cell voltage (V), P is the power density (kW kg^{-1}), and Δt is the discharge time (s).

3. Results and disscussion
3.1 Positive electrode materials

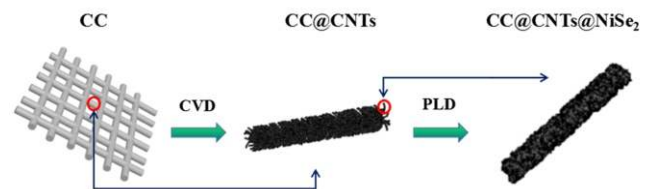The Fig. 1 shows the whole the fabrication procedure of CC@CNT@NiSe₂

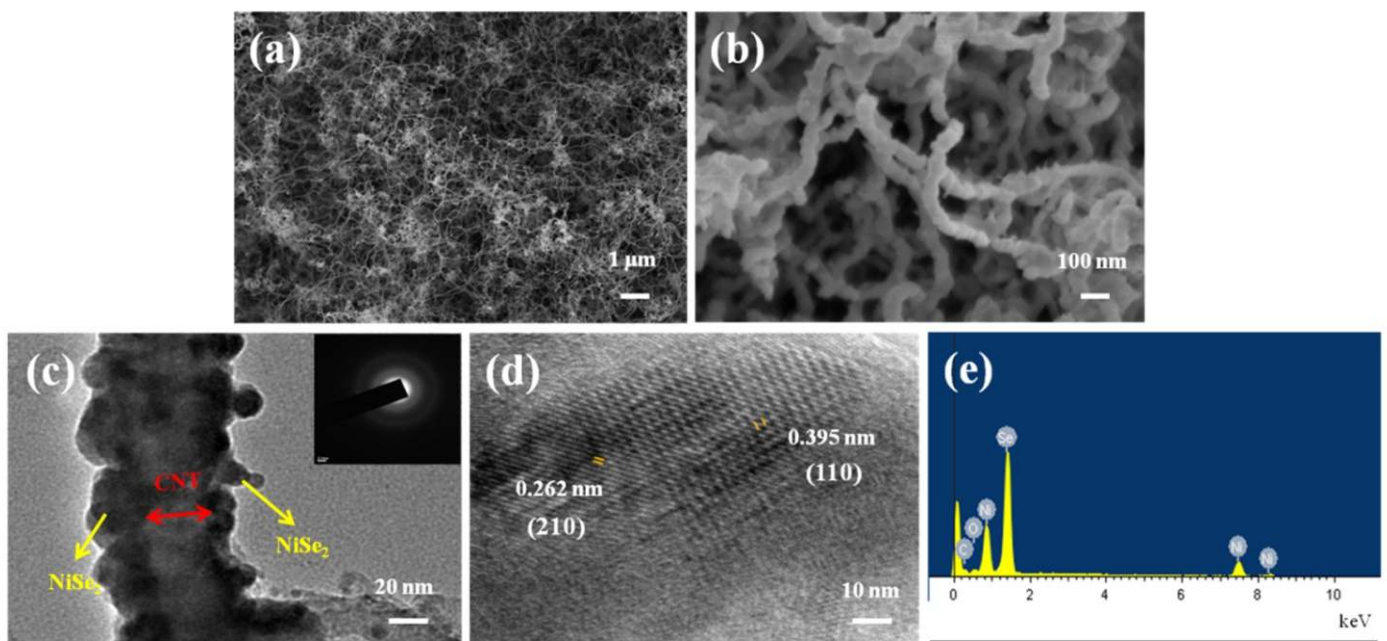**Fig. 1** Schematic illustration of the fabrication procedure of CC@CNT@NiSe₂.

Fig. 2 (a, b) SEM images of CC@CNTs and CC@CNTs@NiSe₂, respectively; (c) TEM images of CC@CNTs@NiSe₂; (d) HRTEM image of CC@CNTs@NiSe₂. (e) EDS of CC@CNTs@NiSe₂.

electrode. The obtained nanostructure and morphology of CC@CNTs@NiSe$_2$ film are exhibited in Fig. 2, which clearly show the CNTs are well-distributed and grown on CC, and the diameter of CNTs is about 20 nm (Fig. 2a). The NiSe$_2$ film was deposited uniformly on the surface of CNTs and the diameter of CC@CNTs@NiSe$_2$ is about 60 nm (Fig. 2b). The as-prepared nanostructure indicates NiSe$_2$ is adhered to the CNTs tightly, which is beneficial to shorten the path of electronic transmission and enhance the conductivity. What's more, CNTs skeleton can avoid the aggregation of NiSe$_2$ and increase contact area with electrolyte, which promote the full implementation of chemical reactions. Therefore, the nanocomposite structure does not easily collapse as the reaction progresses, so that its electrochemical stability is guaranteed.

The CC@CNTs@NiSe$_2$ morphology was further observed by TEM, and the Fig. 2c shows the NiSe$_2$ particles evenly distributed on the surface of CNTs to form a NiSe$_2$ shell. In the high-resolution TEM image (Fig. 2d), the lattice spacing of 0.262 nm and 0.395 nm correspond to (2 1 0) plane and (1 1 0) plane respectively. It reveals that the more active sites of NiSe$_2$ are exposed by PLD, which promotes the occurrence of redox reactions. The EDS element analysis of CC@CNTs@NiSe$_2$ shows that the sample contains C, O, Ni, Se, proving that CC@CNTs@NiSe$_2$ was synthesized successfully by PLD. Raman spectroscopy was used to confirm the bonding environment and molecular structure of NiSe$_2$ and CNTs in CC@CNTs@NiSe$_2$ composite as shown in Fig. 3a. There are four sharp peaks at 140 cm^{-1}, 215 cm^{-1}, 1342 cm^{-1} and 1586 cm^{-1} observed. Notice two sharp peaks at 140 cm^{-1} and 215 cm^{-1} are stretching modes of Se-Se pairs (A$_g$) and the vibration modes of dumbbell-shaped Se–Se pairs (T$_g$), [28] which proves the presence of NiSe$_2$. The peaks of CNTs are at 1342 cm^{-1} and 1589

cm^{-1} corresponding to the D and G bands. The D band is caused by the defects or disorder in carbon and the G band corresponds to the E$_{2g}$ vibration mode of graphite-type sp^2 carbons (Fig. 3b).[29] Compared with CC@CNTs and pure NiSe$_2$, the XRD pattern of CC@CNTs@NiSe$_2$ is similar with CC@CNTs, revealing that NiSe$_2$ film on CC@CNTs obtained by PLD in the room temperature is amorphous.[30]

X-ray photoelectron spectroscopy is a technique for analyzing the chemical properties of the surface, which can evaluate the elemental composition, empirical, elemental chemical state and electronic state in materials. The binding energies of Se 3d at 54.8 and 55.7 eV are assigned to Se3d$_{3/2}$ and 3d$_{5/2}$. The peak at 58.1 eV indicates the oxidized Se in the surface in the Fig. 4a. Fig. 4b shows that there are two peaks attributed to the Ni 2p$_{1/2}$ and Ni 2p$_{3/2}$, which can be resolved into three bands (S1, S2 and S3) (S1*, S2* and S3*) respectively. The S1 (852.3 eV) and S1* (869.2 eV) correspond to Ni^{2+} ions; The S2 (855.2 eV) and S2* (873.1 eV) are assigned to Ni^{3+} ions in the surface oxide phase; The S3 (860.8 eV) and S3* (879.1 eV) show the presence of Ni^{2+} oxidation state.[31]

Fig. 5 shows the results of electrochemical performance of CC@CNTs@NiSe$_2$ systematically by standard three-electrode system and the result was displayed using CV at different scan rates with a potential range from 0 V to 0.5 V (Fig. 5a). It can be seen that the CC@CNTs@NiSe$_2$ electrode has a couple redox peaks due to the pseudocapacitive properties. With increasing the scan rate, the couple redox peaks shift toward corresponding positions, which is due to the polarization effect of the electrode. In addition, there is no significant distortion all the CV curve shapes indicating relatively stable electrochemical performance. Quantitative results can be obtained by charge and discharge tests. Fig. 5b shows the specific capacitances at
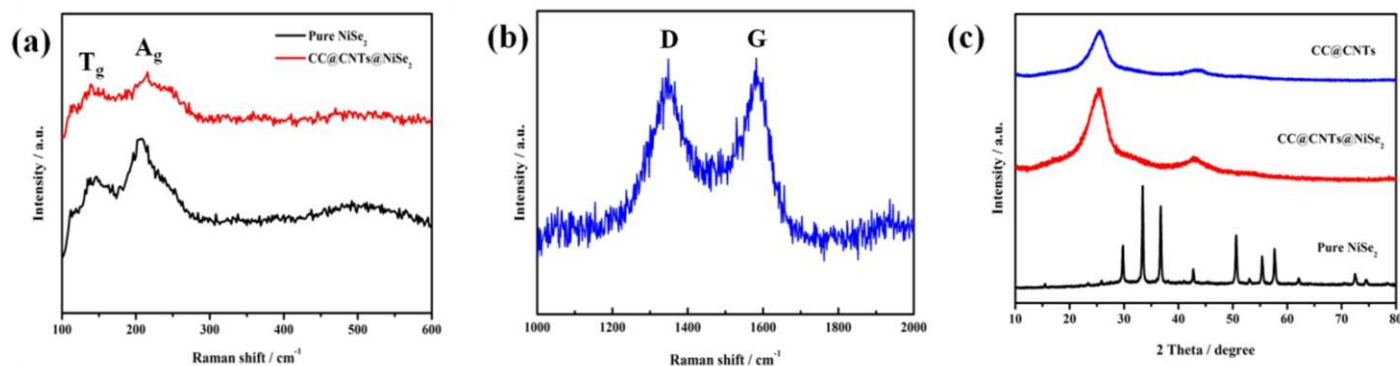

Fig. 3 Raman spectrum (a) CC@CNTs@NiSe$_2$ and pure NiSe$_2$; (b) CNTs of CC@CNTs@NiSe$_2$; (c) XRD of CC@CNTs@NiSe$_2$, CC@CNTs and pure NiSe$_2$.
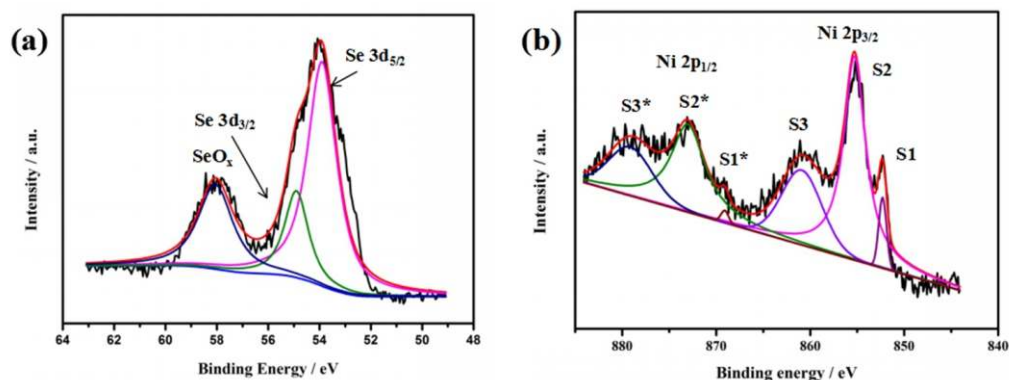

Fig. 4 XPS spectra of CC-CNTs-NiSe$_2$ showing Ni 2p and Se 3d.

different current densities from 2 to 30 A g^{-1}. The CC@CNTs@NiSe$_2$ electrode shows the ideal specific capacitances of 696, 624.5, 542.5, 420 F g^{-1} at 2, 6, 10, 20 A g^{-1} respectively. We can see that the capacitance retention of CC@CNTs@NiSe$_2$ is 60.3 %, when current density increases from 2 to 20 A g^{-1} (Fig. 5c), revealing that the electrode has better rate performance. The results obtained in our work are superior to similar materials reported previously. For example, Lu et al. reported a NiSe$_2$ hollow spheres composite prepared by a hydrothermal method, and the result was 641 and 322 F g^{-1} at 0.5 and 5 A g^{-1} with 50.2% capacitance retention.[14] In addition, the capacitance retention of our composite is 60.3% with current density range from 1 to 20 A g^{-1} that is much better than the performance of NiSe$_2$ hollow spheres composite.

Composite nanostructure of CC@CNTs@NiSe$_2$ electrode is conducive to the rapid Faraday reaction, ensuring the high specific capacitance of the composite. At the same time, highly conductive CNTs support the nanostructure to prevent collapse to promise the better rate performance. Cycle stability is an important performance parameter for supercapacitors. We performed 2000 consecutive charge and discharge tests on CC@CNTs@NiSe$_2$ electrode at a current density of 10 A g^{-1} (Fig. 5d). Initially, there is a significant drop in the capacitance retention the first cycle to the 500th cycle, which is aroused by the loss or dissolution of active materials during the repeated cycling. And then the specific capacitances slowly decreased and hold at 399 F g^{-1}, which are 74 % of the initial specific capacitances. The result shows higher cycle stability than those of previous reports due to the supporting effect of CNTs.

The electrochemical properties of CC@CNTs@NiSe$_2$ obtained by the Decal method and PLD are shown in Fig. 6, which exhibits that the CC@CNTs@NiSe$_2$ prepared by PLD has higher performance than by Decal. The comparison clearly shows that NiSe$_2$ deposited by PLD on CC@CNTs plays excellent synergistic effect which has shorter electron transport channels, more active sites and more stable nanocomposite structure.
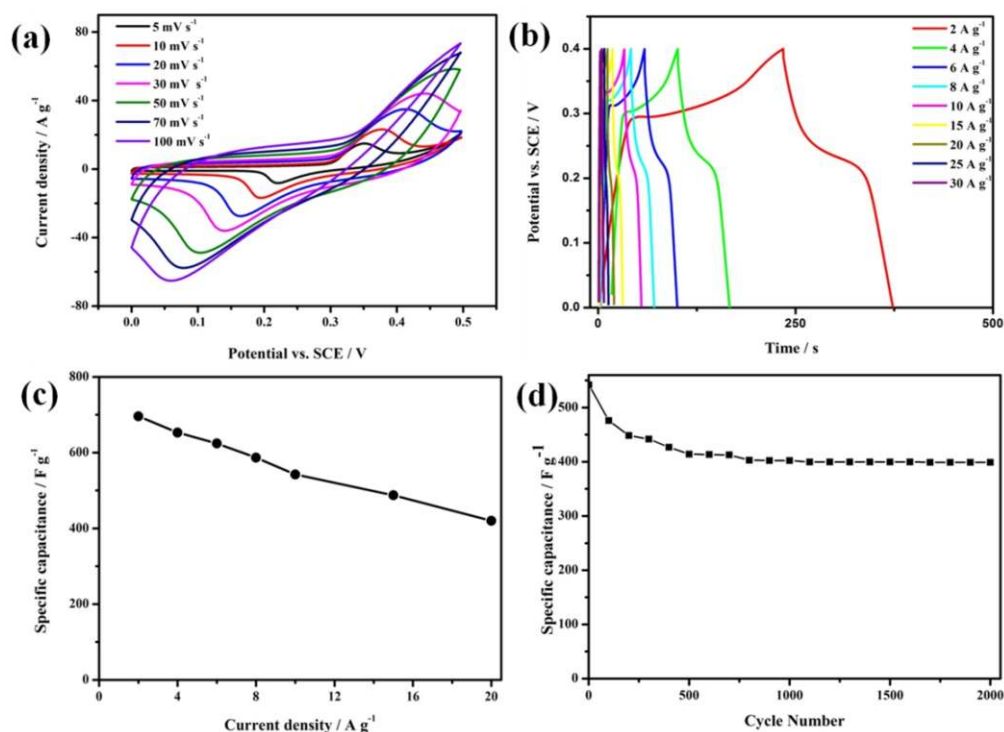

Fig. 5 Electrochemical properties of CC@CNTs@NiSe$_2$. (a) CV curves at different scan rates; (b) GCD curves at different current densities; (c) Specific capacitance at different current densities; (d) Cycling stability plots.
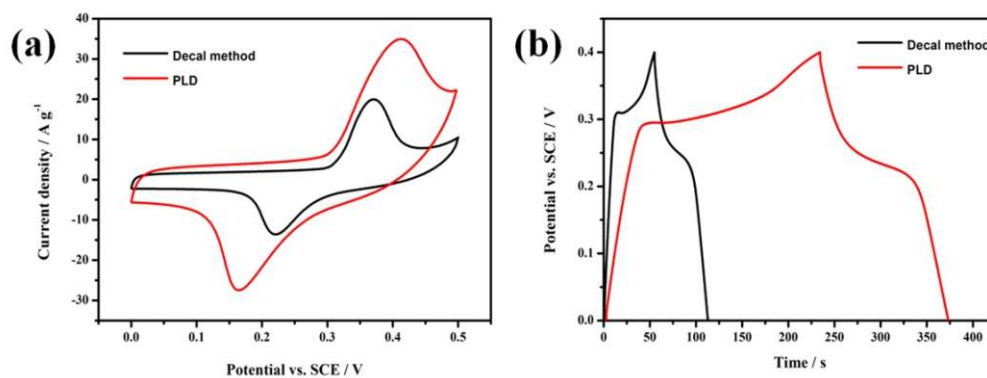

Fig. 6 Electrochemical properties of CC@CNTs@NiSe$_2$ prepared by Decal method and PLD, respectively.

In order to have a deeper understanding of the kinetics factor affected electrochemical performance of CC@CNTs@NiSe$_2$ electrode before and after cycling, the electrochemical impedance spectra (EIS) of CC@CNTs@NiSe$_2$ was tested at 500 mV with the frequency range of 0.1-10^5 Hz. It can be seen that CC@CNTs@NiSe$_2$ showed two parts of a semicircle in a higher frequency region and a straight line at lower frequency. The charge transfer resistance (Rct) corresponds to higher frequency region caused by faradaic redox process.[32] The intercept on real axis in high-frequency region represent the internal resistance (Rs), which reacts the intrinsic resistance of electrode material. The diffusive resistance (Warburg impedance, Z_w) is related to the low frequency region reacting ion diffusion process, showing the impeded diffusion/transport process of electrolyte inside the electrode.[33]
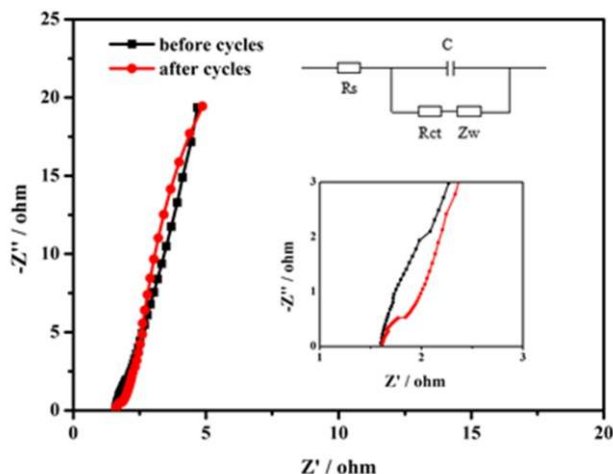

Fig. 6. Nyquist plots of CC@CNTs@NiSe$_2$ in the three-electrode system.

According to the equivalent circuit model, the fitting data was obtained (Table.1). Before and after cycling, as shown in Fig. 6 Rs is nearly unchanged, but Rct and Zw are increased. It's indicated Faradaic reactions is more difficult [34] and ion diffusion inside the electrode is obstructed.[35] The reasons may be due to the morphology change and the increase in impedance, which also are the important factors caused the poor cycling performance.

3.2 Negative electrode materials

In another respect, CNTs were deposited on carbon cloth by CVD as the negative electrode. Carbon cloth is suitable as a carrier due to its flexibility and conductivity.[36] CNTs have excellent conductivity to show good electrochemical performance.[37, 38] SEM and TEM of CC@CNTs were shown in the Fig. 2a and 2c, which details the uniform distribution of CNTs on the CC with the diameter of CNTs is about 20 nm. The electrochemical performance of CC@CNTs was tested in a three-electrode cell system in 1 M KOH aqueous solution. The CV curves (Fig. 7a) measured at different sweep rates (10 to 200 mV s^{-1}) with the potencial range from -1 to 0 V. There is no deformation with the sweep rates of 10 to 200 mV s^{-1} keeping a relatively good rectangular profile. It's proved that CC@CNTs has a typical characteristic of double-layer capacitance. To further illustrate the electrochemical performance, the specific capacitances were calculated quantitatively through the charging and discharging curves at different current densities. We obtain the the specific capacitances of 120, 105.4, 94, 86.4, 81.6 and 65.5 F g^{-1} at 1, 2, 4, 8, 10 and 20 A g^{-1} (54.6 % capacitance retention). It's indicated that CC@CNTs has excellent capacitive behavior and rate capability as a good negative material for ASCs.

3.3 Asymmetric supercapacitors

In order to examine the practical application of CC@CNTs@NiSe$_2$ electrode, an asymmetric supercapacitor was assembled by using
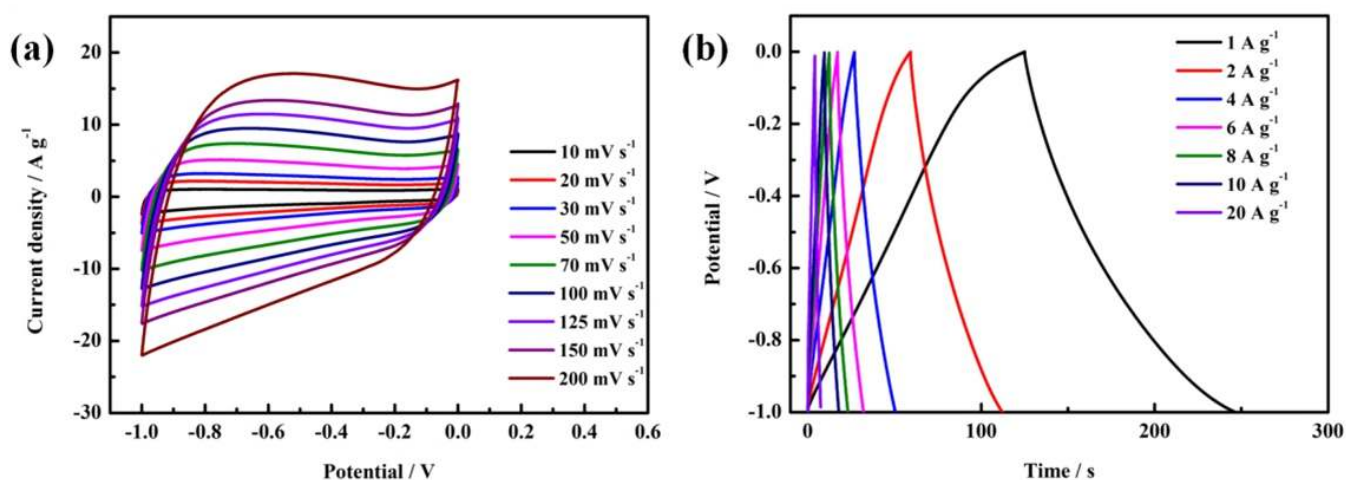

Fig. 7 Electrochemical properties of CC@CNTs. (a) CV curves at different scan rates; (b) GCD curves at different current densities.

Table.1 Comparison of impedance data of CC@CNTs@NiSe$_2$ before and after cycling

Sample	Rs ($\Omega \cdot cm^2$)	Rct ($\Omega \cdot cm^2$)	Zw ($\Omega \cdot s^5 \cdot cm^2$)
Before cycling	1.58	1.66	0.0623
After cycling	1.58	1.85	0.0697

CC@CNTs@NiSe$_2$ and CC@CNTs as the anode and cathode, as shown in Fig. 8a. The active material quality on the positive and negative electrodes can be based on the mass balance method. [39, 40]

$$m_+ / m_- = C_{m-} \Delta V_- / C_{m+} \Delta V_+ \qquad (3)$$

where $+m$, C_{m+} and ΔV_+ are the loading mass (g), specific capacitance (F g^{-1}) and potential (V) of CC@CNTs@NiSe$_2$ electrode; m_- ,C_{m-} and ΔV_- are the loading mass (g), specific capacitance (F g^{-1}) and potential (V) of CC@CNTs electrode, respectively. According to the formula (3),

the mass ratio of positive and negative electrodes is 1:2.[64]

It's obtained that the potential window of 1.3 V is the appropriate potential window based on the different potential window at 20 mV s^{-1} without obvious polarizations (Fig. 8b). The CV curves of the asymmetric supercapacitor have no obvious deformation at different scan rates and show the feature of electric double-layer capacitance and pseudocapacitance (Fig. 8c). The specific capacitance of the asymmetric supercapacitor can be calculated from GCD curves (Fig. 8d). As shown in Fig. 8e, the specific capacitance is 50.77 at 1 A g^{-1} and 29.38 F g^{-1} at 20 A g^{-1}, which shows a capacitance retention is 57.9 %. The long cycle life of CC@CNTs@NiSe$_2$//CC@CNTs asymmetric supercapacitor was
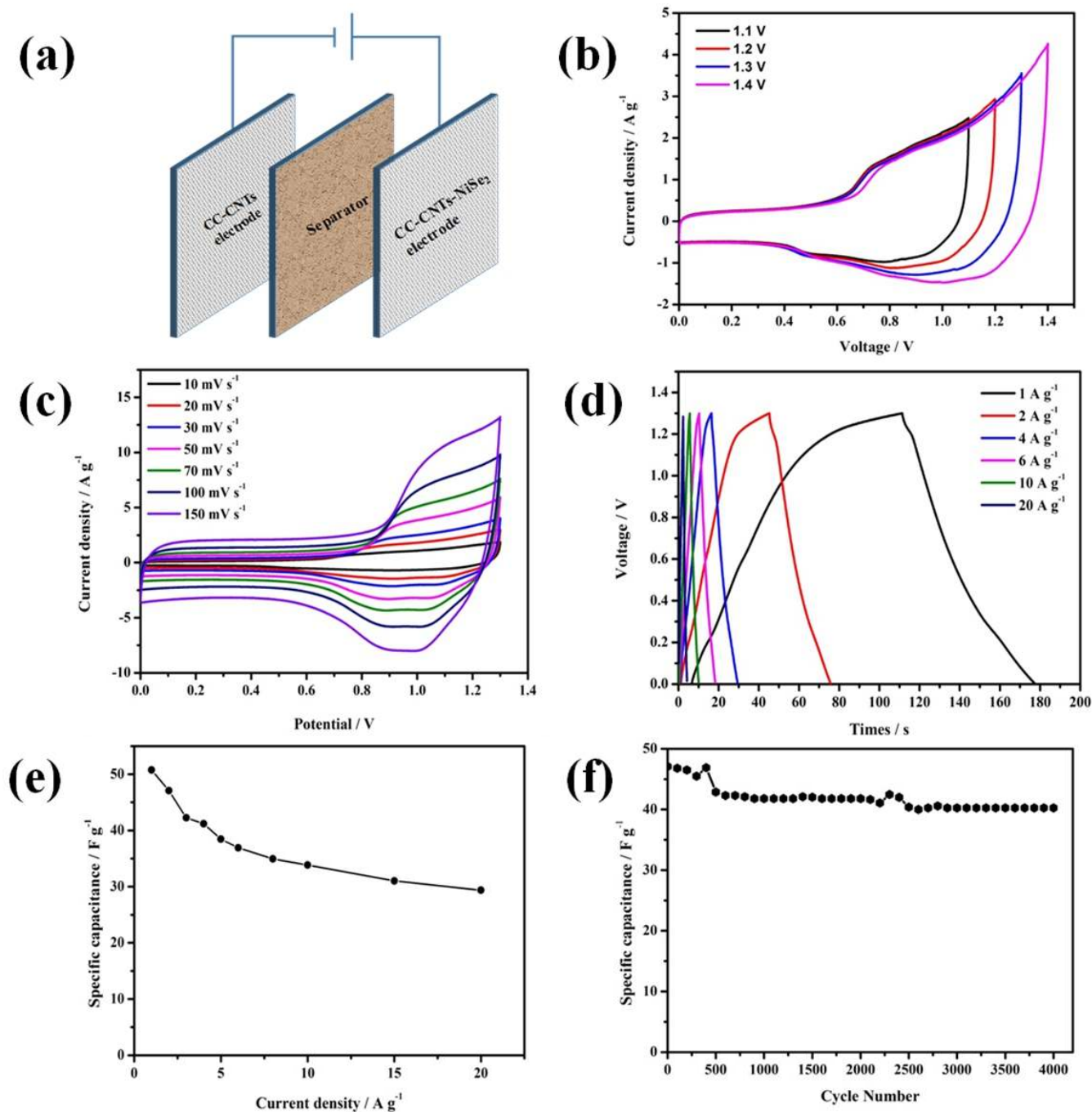

Fig. 8 (a) The schematic illustration of the asymmetric supercapacitor fabrication. Electrochemical performance of CC@CNTs@NiSe$_2$//CC@CNTs asymmetric supercapacitor. (b) CV curves at the different potential window; (c) CV curves at the different scan rates; (d) GCD curves; (e) Rate capability; (f) Cyclic performance.
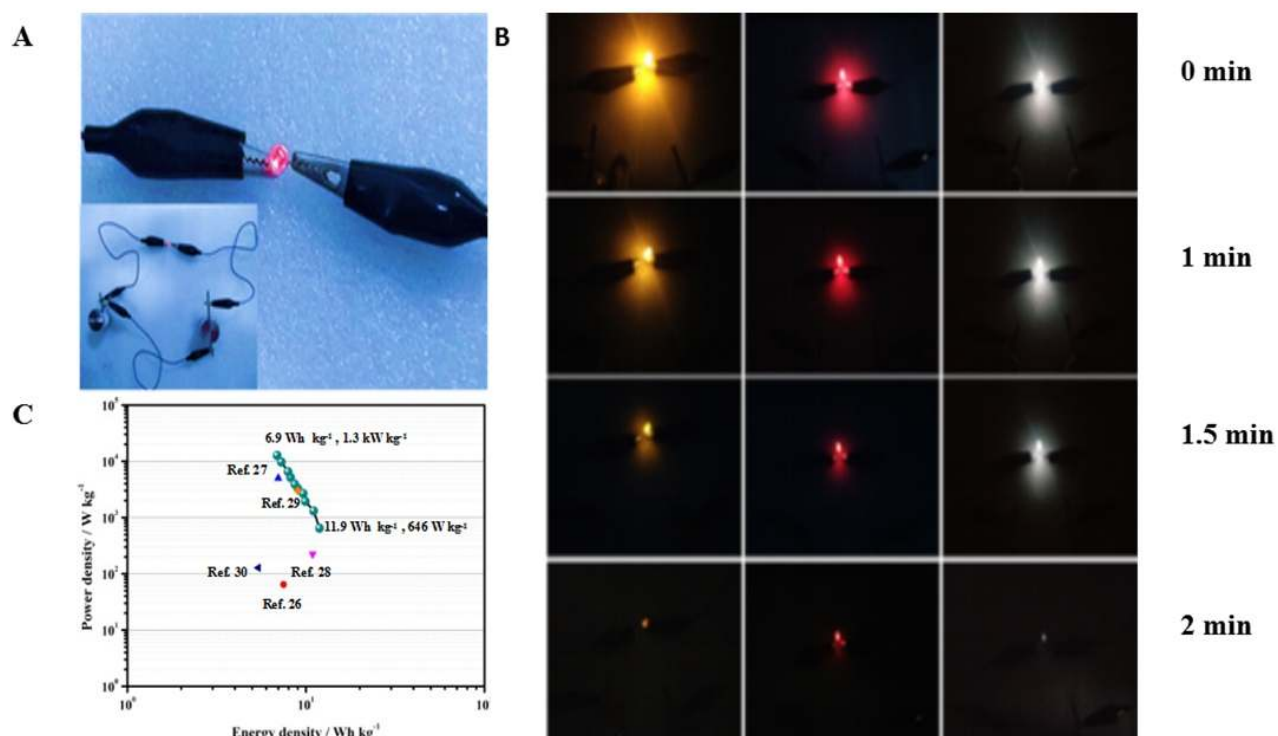
Fig. 9 (A) The device of ASC; (B) The brightness of LEDs in different times; (C) Ragone plot for CC@CNTs@NiSe$_2$//CC@CNTs asymmetric supercapacitor with other related supercapacitors reported previously.

tested at a current density of 3 A g^{-1}. It can be seen that the specific capacitance retention is 85.5 % after 4000 cycles, which is superior to that of single CC@CNTs@NiSe$_2$ electrode and shows the good stability and durability.

According to the formula (1) and (2), the energy density of the ASC are 11.9 Wh kg^{-1} at power density of 646 W kg^{-1} and 6.9 Wh kg^{-1} at power density of 12.7 kW kg^{-1} indicating our ASC has good pseudocapacitive performance and practical prospect. The energy and power densities of present work are higher than reported works, including MCKF@NiO//AC (7.5 Wh kg^{-1})[41], MnO$_2$ nanowire@Graphene//Graphene (7.0 Wh kg^{-1}),[42] nanoporous carbon//nanoporous carbon (10.9 Wh kg^{-1}),[43] Fe$_3$O$_4$@graphene//Fe$_3$O$_4$@graphene (9.0 Wh kg^{-1})[44] and MoS$_2$ nanospheres//MoS$_2$ nanospheres (5.42 W h kg^{-1} at 128 W kg^{-1}).[45] In order to explore the practicality of ASC, the different LEDs were lighted up for 2 min using two ASC devices (Fig. 9B).

4. Conclusions

The CC@CNTs@NiSe$_2$ composite was prepared as the positive electrode materials of supercapacitor. The specific capacitance of CC@CNTs@NiSe$_2$ electrode can reach 696 F g^{-1} at 2 A g^{-1} and 420 F g^{-1} at 20 A g^{-1} (60.3 % retention) respectively. In the long cycling life test, the specific capacitance retention maintained at 74% with 2000 cycles. In order to evaluate the practicality of CC@CNTs@NiSe$_2$ electrode, CC@CNTs@NiSe$_2$//CC@CNTs asymmetric supercapacitor was assembled to measure its electrochemical performance. The energy and power densities of the ASC are 11.9 Wh kg^{-1} and 242 W kg^{-1}, respectively, and the specific capacitance retention is 85.5% , revealing good stability, durability and practicality. The excellent performance of our materials is based on following reasons; (1) With the synergism between NiSe$_2$ and CNTs, CNTs has the excellent conductivity and provides good electron transport channels allowing more fully redox. In addition CNTs has a certain supporting effect on the nanocomposite structure of CC@CNTs@NiSe$_2$, which make the nanocomposite structure more stable and not easy to "collapse" during the reaction process. (2) The CC@CNTs@NiSe$_2$ film prepared by PLD method exposures more active sites that improve electrochemical performance. The CC@CNTs@NiSe$_2$ electrode materials could be promising actual applications for high-performance supercapacitors.

Supporting Information

The Supporting Information is available free of charge on the publications website.

References

1. X. Chen, R. Paul and L. Dai, *Natl. Sci. Rev.*, 2017, **4**, 453-489.
2. P. Fayon, J. M. H. Thomas and A. Trewin, *J. Phys. Chem. C*, 2016, **120**, 25880-25891.
3. G. Yu, X. Xie, L. Pan, Z. Bao and Y. Cui, *Nano Energy*, 2013, **2** , 213-234.
4. X. Xu, W. Shi, W. Liu, S. Ye, R. Yin, L. Zhang, L. Xu, M. Chen, M. Zhong, X. Cao, *J. Mater. Chem. A*, 2018, **6**, 24086.
5. H. Cheng, X. Zhou, A. Gao, F. Yi, D. Shu, X. Song, R. Zeng, C. He, S. Li and D. Zeng, *Electrochim. Acta*, 2018, **292**, 20-30.
6. L. Fan, F. Pan, Q. Tu, Y. Gu, J. Huang, Y. Huang and J. Wu, *Int. J. Hydrogen Energ.*, 2018, **43** , 23372-23381.
7. N. Kaur, E. Comini, D. Zappa, N. Poli and G. Sberveglieri, *Nanotechnology*, 2016, **27**, 205701.
8. B. You and Y. Sun, *Adv. Energy Mater*, 2016, **6**, 1502333.
9. C. Feng, Z. Jin, M. Zhang and Z. S. Wang, *Electrochim. Acta*, 2018, **281**, 237-245.
10. A. M. Abdalla, R. P. Sahu, C. J. Wallar, R. Chen, I. Zhitomirsky and I. K.

Puri, *Nanotechnology*, 2017, **28**, 075603.

11. I. Hasa, R. Verrelli and J. Hassoun, *Electrochim. Acta*, 2015, **173**, 613-618.

12. W. Zhu, X. Yue, W. Zhang, S. Yu, Y. Zhang, and J. Wang, *Chem. commun*., 2016, **52**, 1486-1489.

13. R. Akbarzadeh, H. Dehghani and F. Behnoudnia, *Dalton T.*, 2014, **43**, 16745-16753.

14. M. Lu, X. P. Yuan, X. H. Guan and G. S. Wang, *J. Mater. Chem. A*, 2017, **5**, 3621-3627.

15. M. Z. Xue and Z. W. Fu, *Electrochem. Commun.*, 2016, **8**, 1855-1862.

16. H. Sun, Z. Liang, K. Shen, M. Luo, J. Hu, H. Huang, Z. Zhu, Z. Li, Z. Jiang and F. Song, *Appl. Surf. Sci.*, 2018, **428**, 623-629.

17. K. Guo, S. Cui, H. Hou, W. Chen and L. Mi, *Dalton T.*, 2016, **45**, 19458-19465.

18. N. S. Arul and J. I. Han, *Mater. Lett.*, 2016, **181**, 345-349.

19. S. Wang, W. Li, L. Xin, M. Wu, Y. Long, H. Huang, X. Lou, *Chem. Eng. J.*, 2017, **330**, 1334-1341.

20. R. Wang, P. Sun, H. Wang and X. Wang, *Electrochim. Acta*, 2017, **285**, 876-882.

21. Y. Yang, J. Liu, H. Q. Dai, Y. Cui, J. Liu, X. Liu and Z. W. Fu, *J. Alloy. Compd.*, 2016, **661**, 190-195.

22. S. Kumar, M. Nehra, D. Kedia, N. Dilbaghi, K. Tankeshwar and K. H. Kim, *Prog. Energ.Combu. St.* 2018, **64**, 219-253.

23. Z. Tang, C. H. Tang and H. Gong, *Adv. Funct. Mater.* 2012, **22**, 1272-1278.

24. T. Peng, H. Wang, H. Yi, Y. Jing, P. Sun and X. Wang, *Electrochim. Acta*, 2015, **176**, 77-85.

25. T. Peng, H. Yi, P. Sun, Y. Jing, R. Wang, H. Wang and X. Wang, *J. Mater. Chem. A*, 2016, **4**, 8888.

26. L. Ma, L. Xu, X. Zhou, X. Xu and L. Zhang, *RSC Adv.* 2016, **6**, 91621-91628.

27. J. Balamurugan, C. Li, S. G. Peera, N. H. Kim and J. H. Lee, *Nanoscale*,2017, **9**, 13747-13759.

28. X. Ou, J. Li, F. Zheng, P. Wu, Q. Pan, X. Xiong, C. Yang and M. Liu, *J. Sources*, 2017, **343**, 483-491.

29. C. Li, S. Xu, Y. Yue, B. Yang and X. Wang, *Carbon*, 2016, **103**, 101-108.

30. N. T. Mcdevitt, J. E. Bultman and J. S. Zabinski, *Appl. Spectrosc*., 1998, **52**, 9.

31. B. Wang, X. Wang, B. Zheng, B. Yu, F. Qi, W. Zhang, Y. Li and Y. Chen, *Electrochem. Commun*., 2017, **83**, 51-55.

32. M. Kong, Z. Wang, W. Wang, M. Ma, D. Liu, S. Hao, R. Kong, G. Du, A.M. Asiri, Y. Yao and X. Sun, *Chemistry*, 2017, **23**, 4435-4441.

33. J. Li, H. Xie, Y. Li, J. Liu and Z. Li, *J. Power Sources,* 2011*,* **196**, 10775-10781.

34. X. Yan, X. Tong, J. Wang, C. Gong, M. Zhang and L. Liang, *J. Alloy. Compd,*. 2014, **593**, 184-189.

35. C. Gong, M. Huang, P. Zhou, Z. Sun, L. Fan, J. Lin and J. Wu, *Appl. Surf. Sci.*, 2016, **362**, 469-476.

36. Z. Huang, Z. Zhang, X. Qi, X. Ren, G. Xu, P. Wan, X. Sun and H. Zhang, *Nanoscale*, 2016, **8**, 13273-13279.

37. P. Sun, H. Yi, T. Peng, Y. Jing, R. Wang, H. Wang and X. Wang, *J. Power Sources*, 2017, **341**, 27-35.

38. J. Patiño, N. López-Salas, M.C. Gutiérrez, D. Carriazo, M. L. Ferrer and F. D. Monte, *J. Mater. Chem. A*, 2016, **4**, 1251-1263.

39. W. Kong, C. Lu, W. Zhang, J. Pu and Z. Wang, *J. Mater. Chem. A,* 2015, **3**, 12452-12460.

40. L. Kuang, F. Ji, X. Pan, D. Wang, X. Chen, D. Jiang, Y. Zhang and B. Ding, *Chem. Eng. J.*, 2017, **315**, 491-499.

41. W. Xu, B. Mu and A. Wang, *Electrochim. Acta,* 2016, **194**, 84-94.

42. Z. Wu, W. Ren, D. Wang, F. Li, B. Liu and H. M. Cheng, *ACS Nano*, 2010, **10**, 5835-5842.

43. R. R. Salunkhe, Y. Kamachi, N. L. Torad, S. M. Hwang, Z. Sun, S. X. Dou, J. H. Kim and Y. Yamauchi, *J. Mater. Chem. A*, 2014, **2**, 19848-19854.

44. K. Karthikeyan, D. Kalpana, S. Amaresh and Y. S. Lee, *RSC Adv.*, 2012, **2**, 12322-12328.

45. M. S. Javed, S. Dai, M. Wang, D. Guo, L. Chen, X. Wang, C. Hu and Y. Xi, *J. Power Sources,* 2015, **285**, 63-69.